

DESIGN AND IMPLEMENTATION OF A NANOSATELLITE ATTITUDE DETERMINATION AND CONTROL SYSTEM

**Kristin L. Makovec^{*}, Andrew J. Turner[†],
and Christopher D. Hall[‡]**

The Virginia Tech HokieSat is part of an Air Force initiative for students to design and build satellites. The mission requires an attitude determination and control system (ADCS) that provides adequate control of the spacecraft within a satellite formation, despite its relatively small size and constrained budget, while minimizing power use during flight operations. This paper outlines the development of an ADCS using simple, inexpensive off-the-shelf components and unique algorithms that provide for reliable control over the mission lifetime.

INTRODUCTION

The Virginia Tech HokieSat is one of three satellites flying in the Ionospheric Observation Nanosatellite Formation (ION-F) along with satellites begin built by the University of Washington and Utah State University. This program is part of an initiative funded by the Air Force, DARPA, and the Air Force Research Laboratory (AFRL) to support universities designing and building satellites.

HokieSat is a 15-kg hexagonal satellite with an 18-inch major diameter and a 12-inch height. The satellite will be deployed from the space shuttle in a stack of the three ION-F satellites. These satellites will perform formation flying maneuvers, as well as take measurements of the ionosphere.

This paper presents an in-depth discussion of the HokieSat attitude dynamics and control system (ADCS). An overview of the entire ADCS is given, followed by a closer explanation of the design and implementation of the determination and control

^{*}Graduate Student, Aerospace and Ocean Engineering, Virginia Polytechnic Institute and State University, Blacksburg, Virginia 24061. kmakovec@vt.edu

[†]Graduate Student, Aerospace and Ocean Engineering, Virginia Polytechnic Institute and State University, Blacksburg, Virginia 24061. Member AIAA. ajturner@vt.edu

[‡]Associate Professor, Aerospace and Ocean Engineering, Virginia Polytechnic Institute and State University, Blacksburg, Virginia 24061. Associate Fellow AIAA. Member AAS. cdhall@vt.edu

The ODCS consists of a Global Positioning System (GPS) sensor that provides a state vector to the orbit controller. This position information is compared to the formation flying position as determined from the master controller plan. Due to the fact that HokieSat has a single thrust direction, the ODCS will drive the ADCS in terms of pointing requirements for orbital maneuvers. When there are no ODCS attitude requirements, HokieSat will remain nominally nadir-pointing.

ADCS HARDWARE

The majority of the ADCS hardware for HokieSat is Commercial Off-the-Shelf (COTS). These parts were chosen for various reasons, including ease of implementation, spaceflight heritage, or low cost. In specifying components, the following factors were considered: weight, size, implementation, and cost. Since HokieSat's mass is restricted to 15 kg, each sensor had to be extremely light. Due to the size limits of the spacecraft bus, the component had to fit in a small area, and mount to the structure itself. Since the team consisted of mostly students, the component had to be easily integrated with the spacecraft hardware and electronics with little added work. Lastly, the budget constraints of a student project prevented the use of expensive components. The ADCS hardware locations in the satellite are shown in Figure 2.

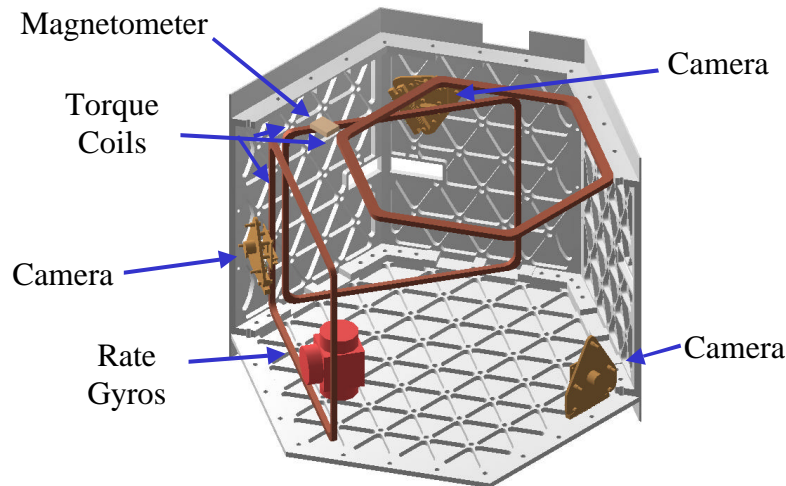


Figure 2 ADCS Component Layout

Attitude Determination Hardware

The attitude determination hardware includes sensors that measure the spacecraft body attitude with respect to inertial space, as well as the spacecraft's angular velocity.

A three-axis magnetometer is used to sense the Earth's magnetic field, \mathbf{B} . This small electronic device senses the \mathbf{B} -field and outputs three voltages, each corre-

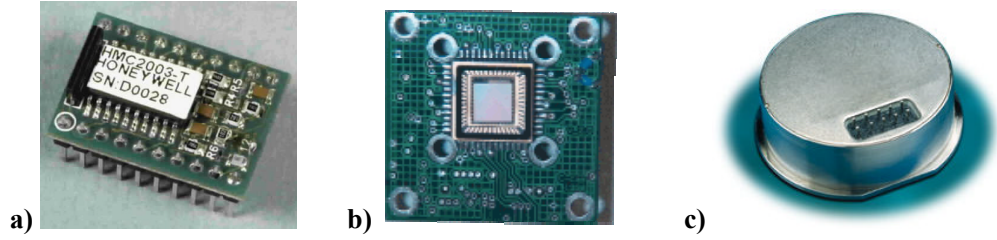


Figure 3 Attitude Determination Hardware: a) Honeywell Magnetometer b) Vector International Camera c) Systron Donner Rate Gyro

sponding to the magnitude along a component axis. This measurement is taken by a low-cost Honeywell HMC-2003 three-axis magnetometer (TAM) (Figure 3(a)) that provides accuracy within 2° . One consideration of using such a sensor is the other inherent magnetic fields in the spacecraft components. Specifically, the antennas and PPT that have a large, quick magnetic field change may cause magnetic field disturbances. This change causes the TAM to become saturated and measure a residual field rather than the actual \mathbf{B} -field. Therefore there is a reset circuit mounted with the TAM that provides a $2\mu\text{s}$ pulse of 3-4 A to clear the circuit. The analog outputs are then measured with an A/D converter for use in the attitude determination algorithm. The inertial \mathbf{B} -field is determined using the IGRF2000 (International Geomagnetic Reference Field) model of the Earth's magnetic field¹ and orbital position from the GPS receiver.

Four Earth-Sun sensing cameras are used to determine a nadir and a Sun vector, and the system is described by Meller, *et al.*² The cameras are located on alternating side panels 120° apart, as well as on the top surface of the satellite. The cameras are Fuga 15d CCDs (Charged Coupled Devices) (Figure 3(b)) manufactured by Vector International and have been used on several spacecraft in the past. They provide black and white digital pictures with a 512×512 pixel resolution. The pictures are analyzed by scanning for horizon lines, as well as for the Sun. The field of view of the lenses is 67° , so there are some gaps in coverage around the spacecraft. These gaps do not degrade the quality of the measurements, however, since each camera is used to detect separate data points and a full representation of the horizon is not required. Due to the configuration, the horizon is in view of at least one camera for all orientations.

The Sun vector is measured by two methods. The first is by using Sun sensing capabilities of the cameras. The second is by measuring the current outputs of the solar arrays based on cosine sun detectors as described by Sidi.³ The current varies by the incidence angle according to the function:

$$i(\alpha) = i(0) \cos \alpha \quad (1)$$

where i is the measured current, $i(0)$ is the maximum current output, and α is the incidence angle measured from orthogonal as shown in Figure 4. The angles are sent to an algorithm to determine a body-fixed sun vector. This is compared with the inertial sun vector as determined using the J2000 Sun model⁴ and telemetry from the orbital position, day of the year and time of day.

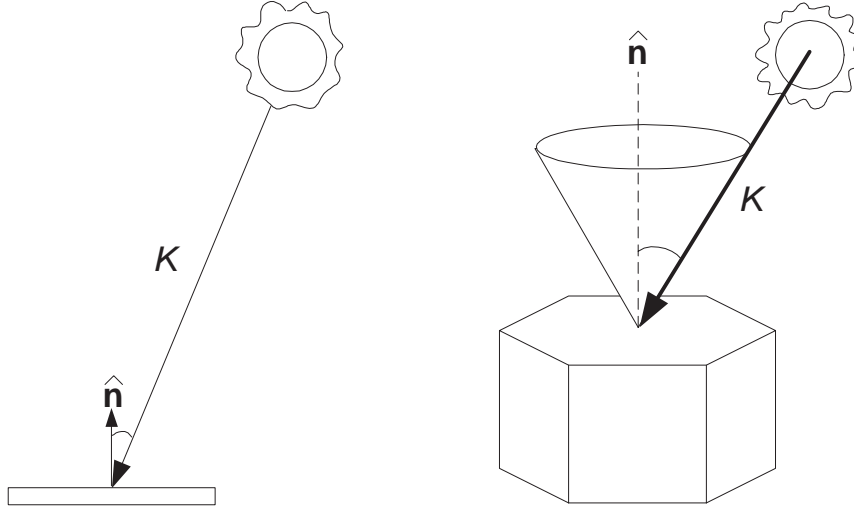


Figure 4 Sun Sensor Detection

Finally, the angular velocity is measured using three solid-state quartz rate sensors. Each sensor measures the angular velocity about a single axis, and together they form a complete angular velocity vector. HokieSat uses the QRS-11 series, produced by BEI Systron Donner Inertial Division (Figure 3(c)). These devices are each only 1.5” in diameter with mass of < 5 g. Together they provide rate measurements with an accuracy of $0.004^\circ/\text{sec}$ which are sent to an A/D Converter on the computer bus.

The components are all relatively inexpensive, as far as spacecraft sensors are concerned, with the rate gyros being the most expensive at approximately \$3,000 each. The attitude determination hardware is summarized in Table 1.

Table 1 SUMMARY OF ATTITUDE DETERMINATION COMPONENTS

Component	Manufacturer	Model	Measurement	Accuracy
Magnetometer	Honeywell	HMC-2003	B -Field	2°
Cameras	Vector International	Fuga 15d	Earth’s Horizon	9°
Solar Arrays	TECSTAR	Solar Cell	Sun Vector	10°
Rate Sensor	BEI Systron Donner	QRS-11	Angular Velocity	$0.004^\circ/\text{s}$

Attitude Control Hardware

For attitude control, HokieSat uses three magnetic torque coils which are oriented orthogonally to each other. These are constructed in-house from coils of copper magnet wire covered with epoxy for stiffness, and then wrapped in KaptonTM tape. These coils provide a torque when a current is passed through the loop, and each coil is capable of producing a magnetic moment of 0.9 A-m².

The torque coils are sized in a tradeoff between minimizing power and mass, and maximizing the magnetic moment output. These characteristics are related by:

$$M = INA_c \quad (2)$$

where I is the applied current, N is the number of turns of wire, and A_c is the area of the coil.⁵ This equation can be rearranged to obtain the number of turns of wire required as a function of magnetic moment, power, coil size, and wire characteristics:

$$N = \frac{4M^2 p_c \hat{R}}{PA_c^2 \pi d_w^2} \quad (3)$$

where p_c is the perimeter of the coil, \hat{R} is the resistivity of copper, P is the power required, and d_w is the diameter of the wire.

On HokieSat, there is one hexagonal coil with 80 turns of wire on the top face with an inside major radius of 5.69 inches. There are two rectangular coils with 133 turns of wire located adjacent to side panels, which are mutually orthogonal. The rectangular coils have inner dimensions of 7 × 9 inches. By allocating 0.75 W for torque coil control, each coil develops up to 0.9 Am². A 24-gauge magnet wire is used with a value of \hat{R} of $1.7 \times 10^{-8} \Omega\text{m}$.

The hardware characteristics of the attitude determination and control system are summarized in Table 2.

Table 2 ADCS HARDWARE CHARACTERISTICS

Component	Mass (g)	Voltage (V)	Power (W)
Magnetometer	69	15.0	0.30
Cameras	381	5.0	0.20
Rate Sensor	232	5.0	3.60
Torque Coils	570	3.3	0.75

ATTITUDE DETERMINATION ALGORITHMS

A suitable set of attitude determination algorithms was developed to satisfy the requirements set forth by the mission success specifications. Since we are using in-

expensive components, we sacrifice some accuracy on each sensor. Therefore, the algorithms must be able to account for these inaccuracies and use the over-determined solution to minimize the final attitude error.

Another difficulty with a nanosatellite system is the largely fluctuating amount of available power for the determination hardware. At certain times in the orbit some sensors must be deactivated and reactivated as power allotment allows. The determination algorithms account for this by using several different schemes when mixing the sensor information to obtain an accurate final solution.

The three cases are:

Case 1 Rate gyros and more than one sensor available

Case 2 Rate gyros and one sensor available

Case 3 Rate gyros not available

Case 1: Rate gyros and more than one sensor available (Figure 5): The multiple vector measuring sensors are first reduced using the QUEST least-squares single frame optimal estimator. The resulting quaternion is then passed, along with the rate gyro measurements, to an extended Kalman filter (EKF, adapted from Lefferts, *et al.*⁶ by T. Humphreys at Utah State University). This method provides an attitude measurement of $< 1^\circ$ absolute angle error.

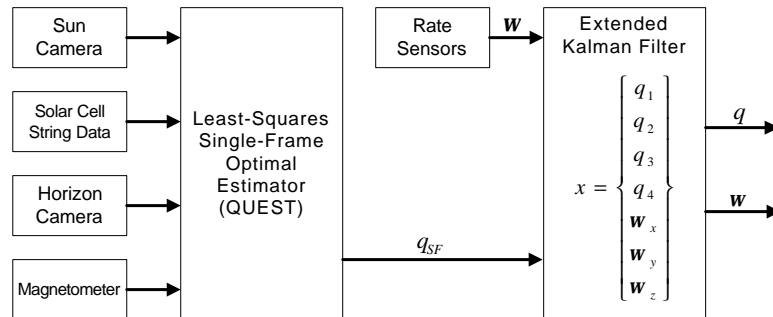


Figure 5 Determination Case 1: Rate Gyros and More Than One Sensor Available

Case 2: Rate Gyros and one sensor available (Figure 6): The result of decreased sensor measurements from Earth eclipse or unavailable data will require a mode in which only the magnetometer and rate gyro information are used. With only rate and magnetometer data available, state observability is reduced. The Kalman Filter takes longer to converge and accuracy is decreased. This method provides an attitude measurement of $< 5^\circ$ absolute angle error.

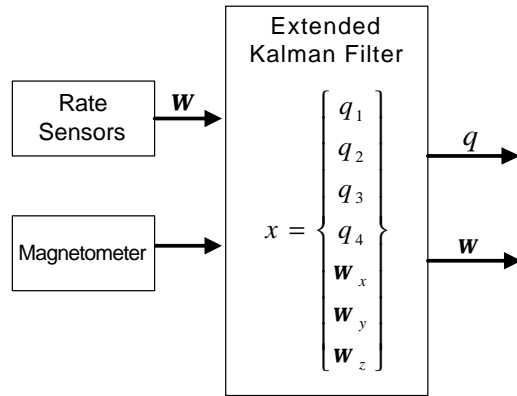


Figure 6 Determination Case 2: Rate Gyros and One Sensor Available

Case 3: Rate gyros not available (Figure 7): The last case is a result of low power. Since the rate gyro consumes approximately 24% of system power, there are times (such as eclipse) when the angular rate is unknown. Therefore, there exists a case to use the remaining vector sensors to determine an accurate attitude measurement. The EKF for this case must operate without an angular rate input. This method has been adapted from Bar-Itzhack and Oshman.⁷ The estimated accuracy is 1-10° absolute angle error, depending on the actual available sensors.

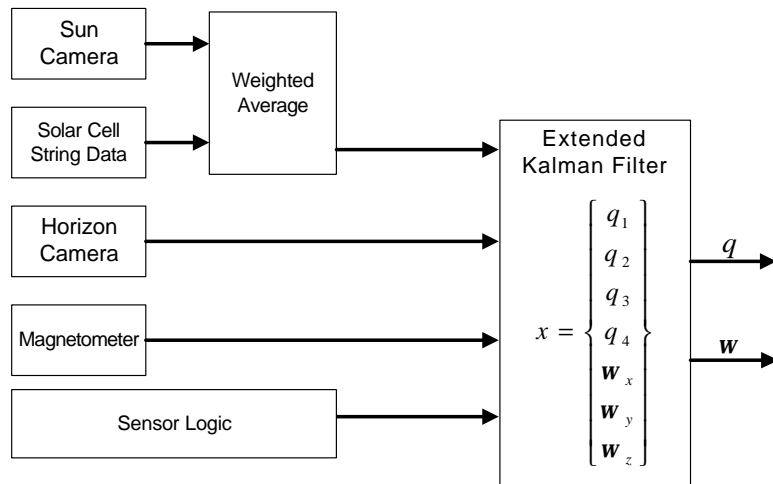


Figure 7 Determination Case 3: Rate Gyros Not Available

The QUEST algorithm is used to determine an attitude estimate from the multiple sensor measurements. The algorithm fuses the body measurement vectors and the known inertial vectors for each sensor measurement. However, the standard QUEST

algorithm leads to singularities with rotations of π . Therefore, sequential rotations as developed by Shuster and Oh⁸ are used to alleviate this problem with little overhead calculation.

CONVENTIONAL CONTROL ALGORITHMS

A constant coefficient linear quadratic regulator is used to determine the magnetic control applied to the spacecraft. This study is based on the work of Musser and Ebert,⁹ Wiśniewski,^{10,11} and Makovec.¹²

Equations of Motion

The nonlinear equations of motion for an orbiting spacecraft are

$$\dot{\boldsymbol{\omega}} = -\mathbf{I}^{-1}\boldsymbol{\omega}^\times\mathbf{I}\boldsymbol{\omega} + 3\omega_c^2\mathbf{I}^{-1}\hat{\mathbf{o}}_3^\times\mathbf{I}\hat{\mathbf{o}}_3 + \mathbf{I}^{-1}\mathbf{g}_m \quad (4)$$

and

$$\dot{\bar{\mathbf{q}}}^{bi} = \frac{1}{2} \begin{bmatrix} \mathbf{q}^{bi\times} + q_4^{bi}\mathbf{1} \\ -\mathbf{q}^{biT} \end{bmatrix} \boldsymbol{\omega} \quad (5)$$

where $\bar{\mathbf{q}}^{bi}$ is the quaternion describing the orientation of the body frame with respect to the inertial frame, $\boldsymbol{\omega}$ is the angular velocity of the body frame with respect to the inertial frame, ω_c is the orbital mean motion, \mathbf{I} is spacecraft moment of inertia, $\hat{\mathbf{o}}_3$ is the nadir vector, and \mathbf{g}_m is the magnetic torque. Note that $\hat{\mathbf{o}}_3$ is the third column of \mathbf{R}^{bo} , which is the rotation matrix describing the orientation of the body frame with respect to the orbital frame. The quaternion corresponding to \mathbf{R}^{bo} is denoted $\bar{\mathbf{q}}^{bo}$, and the angular velocity of the body frame with respect to the orbital frame is denoted $\boldsymbol{\omega}^{bo}$.

For three-axis stability, the body frame should be aligned with the orbital frame, or

$$\boldsymbol{\omega}^{bo} = \mathbf{0} \quad (6)$$

$$\bar{\mathbf{q}}^{bo} = \begin{bmatrix} \mathbf{0} \\ 1 \end{bmatrix} \quad (7)$$

These equations imply that the spacecraft nadir vector always points to the center of the Earth.

Linear time-varying equations are obtained in quaternion form by linearizing around the desired equilibrium point. The equations of motion follow the linear state equation

$$\dot{\mathbf{x}} = \mathbf{F}\mathbf{x} + \mathbf{G}(t)\mathbf{M}(t) \quad (8)$$

where \mathbf{F} is the system matrix of linearized equations, $\mathbf{G}(t)$ is the input matrix, and $\mathbf{M}(t)$ is the applied control in the form of magnetic moment. The state vector, \mathbf{x} ,

contains the vector portion of the quaternions and their rates of change from Eq. 5, or

$$\mathbf{x} = \begin{bmatrix} \mathbf{q} \\ \dot{\mathbf{q}} \end{bmatrix} \quad (9)$$

Using small angle assumptions, the linearized equations of motion are:

$$\dot{\mathbf{x}} = \mathbf{F}\mathbf{x} + \mathbf{I}^{-1}\mathbf{g}_m \quad (10)$$

where

$$\mathbf{F} = \begin{bmatrix} 0 & 0 & 0 & 1 & 0 & 0 \\ 0 & 0 & 0 & 0 & 1 & 0 \\ 0 & 0 & 0 & 0 & 0 & 1 \\ -4\omega_c^2\sigma_1 & 0 & 0 & 0 & 0 & \omega_c - \omega_c\sigma_1 \\ 0 & 3\omega_c^2\sigma_2 & 0 & 0 & 0 & 0 \\ 0 & 0 & \omega_c^2\sigma_3 & -\omega_c - \omega_c\sigma_3 & 0 & 0 \end{bmatrix} \quad (11)$$

Here,

$$\sigma_1 = \frac{I_2 - I_3}{I_1} \quad \sigma_2 = \frac{I_3 - I_1}{I_2} \quad \sigma_3 = \frac{I_1 - I_2}{I_3} \quad (12)$$

The magnetic control portion of the equations of motion is

$$\mathbf{I}^{-1}\mathbf{g}_m = \mathbf{G}(t)\mathbf{M}(t) \quad (13)$$

where

$$\mathbf{g}_m = \mathbf{M}^\times \mathbf{B} \quad (14)$$

\mathbf{B} is the magnetic field, and \mathbf{M} is the magnetic moment. Since the magnetic torque must be perpendicular to the magnetic field, the following mapping function can be used for \mathbf{M} as suggested by Wiśniewski:^{10,11}

$$\tilde{\mathbf{M}} \mapsto \mathbf{M} : \mathbf{M} = \frac{\tilde{\mathbf{M}}^\times \mathbf{B}}{\|\mathbf{B}\|} \quad (15)$$

This relation ensures that \mathbf{M} is perpendicular to the magnetic field by determining a mapped magnetic moment, $\tilde{\mathbf{M}}$, of the same magnitude, which is the ideal desired torque. When crossed into the magnetic field, the mapped magnetic moment provides a feasible control magnetic moment by selecting the component of $\tilde{\mathbf{M}}$ perpendicular to the magnetic field. This mapping leads to an input control matrix, $\mathbf{G}(t)$ of

$$\mathbf{G}(t) = \frac{-\mathbf{I}^{-1}}{\|\mathbf{B}\|} \mathbf{B}^\times \mathbf{B}^\times = \frac{-\mathbf{I}^{-1}}{\|\mathbf{B}\|} \begin{bmatrix} -B_y^2 - B_z^2 & B_x B_y & B_x B_z \\ B_x B_y & -B_x^2 - B_z^2 & B_y B_z \\ B_x B_z & B_y B_z & -B_x^2 - B_y^2 \end{bmatrix} \quad (16)$$

where the magnetic field, \mathbf{B} , is in the body frame.

Linear, time-invariant equations of motion are obtained by exploiting the periodic nature of the system. The $\mathbf{G}(t)$ matrix is dependent only upon the moments of inertia of the spacecraft, which are constant in the body frame, and the magnetic field. The magnetic field is roughly periodic with orbital period, leading to a roughly periodic $\mathbf{G}(t)$. The relation

$$\mathbf{G}(t + \mathcal{T}) = \mathbf{G}(t) \quad (17)$$

is approximately valid over several orbits.

The time-varying parameters in the magnetic torque component of the equations of motion are replaced with their average values so there is no dependence on time. The average value of $\mathbf{G}(t)$ is $\bar{\mathbf{G}}$ where

$$\bar{\mathbf{G}} = \frac{1}{\mathcal{T}} \int_0^{\mathcal{T}} \mathbf{G}(t) dt \quad (18)$$

and \mathcal{T} is the period of the orbit. Thus,

$$\dot{\mathbf{x}} = \mathbf{F}\mathbf{x} + \bar{\mathbf{G}}\mathbf{M} \quad (19)$$

is a linear time-invariant model for the system.

Control Laws

A constant coefficient linear quadratic (LQR) controller is used to stabilize the system with magnetic control. The magnetic control is set equal to

$$\tilde{\mathbf{M}}(t) = -\mathbf{K}\mathbf{x}(t) \quad (20)$$

where \mathbf{K} is the gain feedback matrix. The controller gain, \mathbf{K} , is calculated using the steady-state solution to the Ricatti equation

$$-\dot{\mathbf{S}} = \mathbf{S}\mathbf{F} + \mathbf{F}^T\mathbf{S} - (\mathbf{S}\bar{\mathbf{G}})^{-1}\mathbf{B}\bar{\mathbf{G}}^T\mathbf{S} + \mathbf{Q} \quad (21)$$

where \mathbf{Q} is defined as a diagonal weight matrix. A linear quadratic regulator is used to calculate the optimal gain matrix for the time-invariant linear system. The gain matrix is equal to

$$\mathbf{K} = -\mathbf{B}^{-1}\bar{\mathbf{G}}^T\mathbf{S} \quad (22)$$

and thus

$$\tilde{\mathbf{M}}(t) = -\mathbf{B}^{-1}\bar{\mathbf{G}}^T\mathbf{S}(t)\mathbf{x}(t) \quad (23)$$

This controller is implemented in Eqs. 13 and 15.

Floquet's theory describes dynamic systems in which the coefficients are periodic.¹³ This theory is directly applicable to the magnetic control problem. After the controller gain is calculated for the time-invariant linear system, the stability of the linear time-varying system is examined using Floquet's theory.

For stability, \mathbf{Q} must be chosen through trial and error such that the eigenvalues of $\mathcal{X}(\mathcal{T})$ are located inside the unit circle, where

$$\mathcal{X}(\mathcal{T}) = [\mathbf{x}_1(\mathcal{T}) \quad \mathbf{x}_2(\mathcal{T}) \quad \cdots \quad \mathbf{x}_6(\mathcal{T})] \quad (24)$$

is obtained using initial values

$$\mathcal{X}(0) = [\mathbf{x}_1(0) \quad \mathbf{x}_2(0) \quad \cdots \quad \mathbf{x}_6(0)] = \mathbf{I}_{6 \times 6} \quad (25)$$

With the control gain matrix known, the linear system

$$\dot{\mathbf{x}} = \mathbf{F}\mathbf{x} - \mathbf{G}(t)\mathbf{K}\mathbf{x} \quad (26)$$

is solved. The mapped magnetic moment is solved using Eq. 20, and the applied magnetic moment is calculated from the mapping function in Eq. 15. This magnetic moment is implemented in the linear system in Eq. 10.

The constant gain matrix determined from the linear quadratic regulator can be implemented in the nonlinear system. However, since these gains were formed using the linear time-invariant system and optimized for use in the linear time-varying system, there is no guarantee that the nonlinear system will be stable. The results from each nonlinear simulation must be individually examined to check for stability.

This process is summarized in Figure 8.

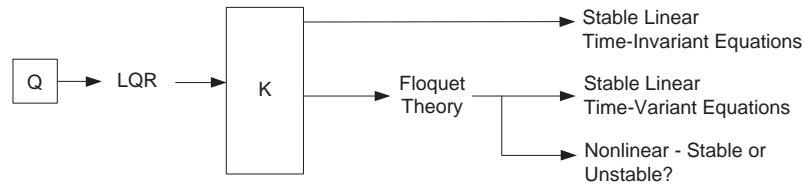


Figure 8 Summary of LQR Controller Method

Simulation Results

Simulations are performed using Matlab. For all spacecraft configurations studied here, there are choices of \mathbf{Q} which lead to gains that bring the spacecraft to the desired equilibrium orientation. It is possible to stabilize the system regardless of the presence or absence of inherent gravity-gradient stability.

The linear time-varying equations are always stable if the eigenvalues of the $\mathcal{X}(t)$ matrix are located in the unit circle, but the nonlinear system is not necessarily stable with the same gains. Results from each set of gains must be individually examined to check for stability of the nonlinear equations. If the nonlinear equations are not stable, new \mathbf{Q} values are implemented and checked.

The quaternion resulting from the implementation of the linear quadratic regulator controller for a gravity-gradient stable spacecraft is shown in Figure 9(a). The magnetic moment required for spacecraft stability is determined in the simulation, and can be adjusted by altering the gains. There is a tradeoff between the required magnetic moment and the time required to stabilize. The magnetic moment required to stabilize the system in Figure 9(a) is shown in Figure 9(b).

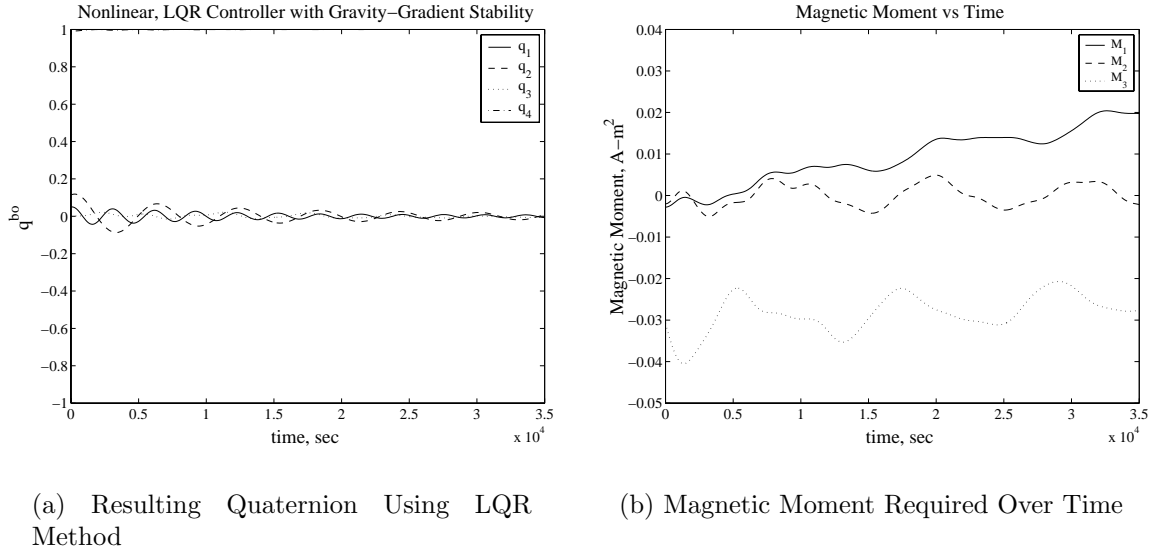


Figure 9 Results From Implementation of LQR Controller

The magnetic moment required experiences long period oscillations over time. These oscillations are evident when the magnetic moment is plotted over a long period of time in Figure 10. In this case, one period is equal to approximately six days, and this periodic nature occurs because of the relative rotation between the Earth spin axis and the magnetic field, coupled with the orbital position of the spacecraft.

Spacecraft occasionally become inverted upon deployment from their launch vehicles, so knowing if the attitude control system can flip the satellite is desirable. A non gravity-gradient stable spacecraft is examined with a rotation 179° out of plane from nadir pointing. Values of the weight matrix, \mathbf{Q} , are determined that can obtain the correct attitude for the inverted spacecraft. The resulting quaternion is shown in Figure 11(a), and the amount of magnetic moment that is required is shown in Figure 11(b).

ADAPTIVE CONTROL ALGORITHMS

Another approach to determining the appropriate controls is through the use of an adaptive algorithm.¹⁴ This type of controller will adapt over time to find control maneuvers that minimize time and energy despite a changing environment. Neural

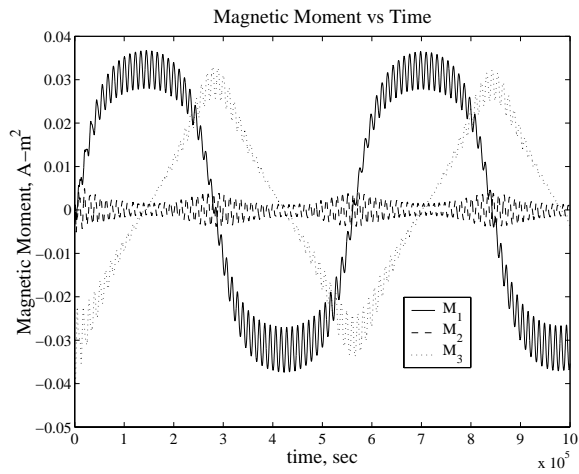
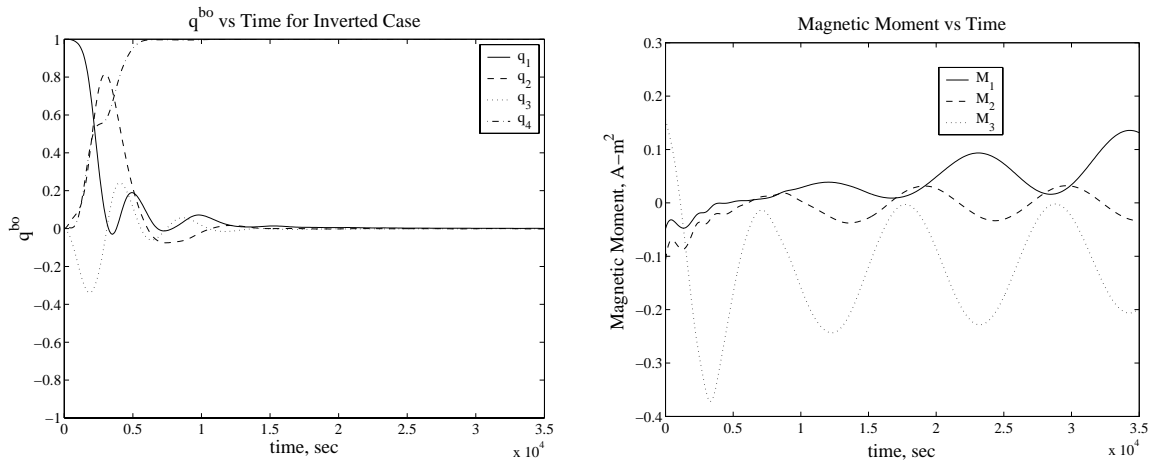


Figure 10 Periodic Nature of Magnetic Moments



(a) Resulting Quaternion Using LQR Method with Inverted Spacecraft

(b) Magnetic Moment Required Over Time with Inverted Spacecraft

Figure 11 Results From Implementation of LQR Controller with Inverted Spacecraft

networks have been used in many nonlinear control applications, but only recently have been proposed for spacecraft control.¹⁵⁻¹⁷

An adaptive control system, shown in Figure 12, can greatly enhance the mission success of a spacecraft by possibly providing the best possible control of the satellite regardless of previous system knowledge. This enhanced independent control is especially true when ground communications is limited, as is the case for HokieSat. The satellite must be able to continue mission operations autonomously despite changes in the spacecraft system.

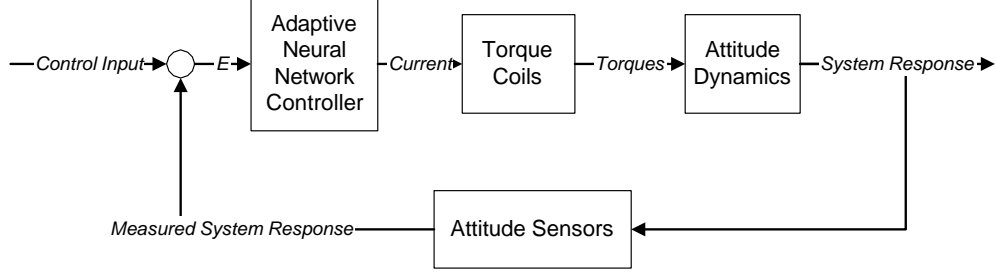


Figure 12 Adaptive Network Control Loop

There are many unknowns that are not accounted for when designing conventional control algorithms such as non-rigidity, accurate atmospheric effects, and changes in the system like a malfunctioning torque coil. The adaptive controller accounts for these unknowns by comparing the expected system response with the actual system response and updating its internal model. This updating is done by computing the error as shown in Eq. 27.

$$E^T = \frac{1}{2} \sum_j (y_{\tau,j}^T - y_{\tau,j})^2 = \frac{1}{2} \sum_j e_{\tau,j}^2 \quad (27)$$

where the subscript j denotes the number of distinct plant outputs, and $y_{\tau,j}^T$ and $y_{\tau,j}$ respectively represent the j th desired target and the j th actual plant output at time τ .

The controller employs a neural network (NN), shown in Figure 13, to determine the appropriate controls. This network contains synaptic weights, like gains, that can be updated to obtain a better solution. For the attitude controller, the set of inputs $(\mathbf{q}, \boldsymbol{\omega}, \dot{\boldsymbol{\omega}})$ is defined as the state vector \mathbf{x} . For each layer, there is a vector of weights, w_i , and a bias vector, b_i , where i is the corresponding layer. The basic neural network equation then looks like:

$$\mathbf{g} = w_2[\tanh(w_1\mathbf{x} + b_1)] + b_2 \quad (28)$$

where \mathbf{g} is the desired control moment, and the output of the neural network that uses \tanh as the squashing function to limit saturation.

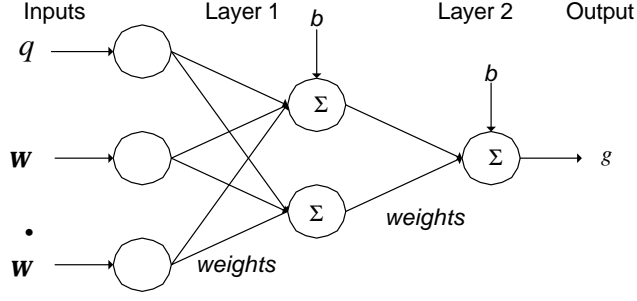


Figure 13 Example of a Neural Network

The weight updates are determined by a gradient method based on the measured system response error:

$$w_{ij}(\tau + 1) = w_{ij}(\tau) - \eta \frac{\partial E^T}{\partial w_{ij}(\tau)} + \alpha \Delta w_{ij}(\tau - 1) \quad (29)$$

where η is the design specified learning rate, α is the momentum factor, and τ indicates the number of training iterations. The momentum factor is used to allow the neural network to continue updating the weights due to a previous iteration's error. This momentum helps keep the network output smooth and react less to erroneous changes within a single iteration. Both η and α are chosen by the system designer and are specific to the application.

Applying this weight update to the control system, the neural network acts as a model of the spacecraft. The system is then inverted to create a predictor for the control signals based on the desired attitude. This Neural Network Model Reference Controller (NNMRC) is shown in Figure 14.¹⁸ The expected system response, \hat{y} , is determined by evaluating the neural network:

$$\hat{y}(t + 1) = w_2 [\tanh(w_1 \mathbf{u} + b_1)] + b_2 \quad (30)$$

The neural network is then inverted to determine the appropriate control signal, u , based on the desired output, \bar{y} , and the error of the previous system response, e .

$$e(t + 1) = \bar{y}(t) - (y(t) - \hat{y}(t)) \quad (31)$$

$$u(t + 1) = u(t) + \eta e(t + 1) w_2 [\operatorname{sech}^2(w_1 p + b_1)] w_1 \frac{dp}{du} \quad (32)$$

where p is the state vector and the control input vector, $\begin{bmatrix} x \\ \hat{y} \end{bmatrix}$. The disturbances shown in Figure 14, d , are unknown external forces that affect the system. The NN

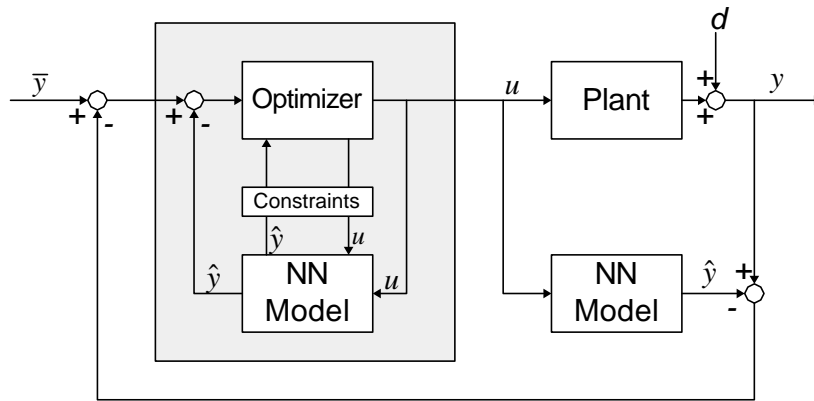


Figure 14 Neural Network Model Reference Controller

model is updated as the spacecraft is controlled, and subsequently the system response error decreases with time. By having no *a priori* knowledge of the spacecraft plant, the NN model has no predilection to the assumed system, but merely learns how to control the actual system.

In practice, HokieSat will employ the conventional control algorithms for most of the mission lifetime. During normal operations, the adaptive control system will update its NN model, and predict possible control torques. These calculated moments will be monitored from the ground and be used to assess the quality of the adaptive controller before it is put online.

CONCLUSIONS

The HokieSat attitude determination and control system (ADCS) is a complete system that provides accurate, reliable information on the attitude of the nanosatellite, as well as enables robust control in completing the Ionospheric Observation Nanosatellite Formation (ION-F) mission. The presented ADCS can be applied for general use to almost any low-cost, small satellite system.

Conventional control provides a good, reliable means of determining control moments for the spacecraft and can be updated using the supplied techniques. Furthermore, adaptive algorithms can be added to allow for unexpected changes to the system and continue to provide robust control during mission operations.

ACKNOWLEDGEMENTS

This project has been supported by the Air Force Research Laboratory, the Air Force Office of Scientific Research, the Defense Advanced Research Projects Agency, NASA Goddard Space Flight Center, and the 3 universities. We especially acknowledge the efforts of many of the students on the HokieSat, USUSat, and Dawgstar

teams who have contributed to the development of the ADCS components and algorithms. Orbital Sciences Corporation provided invaluable advice on practical issues of ADCS design and implementation.

REFERENCES

- [1] Division V, Working Group 8, *International Geomagnetic Reference Field - 2000*, International Association of Geomagnetism and Aeronomy (IAGA), 2000.
- [2] Meller, D., Sripruetkiat, P., and Makovec, K., “Digital CMOS Cameras for Attitude Determination,” *Proceedings of the 14th AIAA/USU Conference on Small Satellites, Logan, Utah*, August 2000, pp. 1–12, SSC00-VII-1.
- [3] Sidi, M. J., *Spacecraft Dynamics and Control, A Practical Engineering Approach*, Cambridge Aerospace Series, Cambridge University Press, Cambridge, 1997.
- [4] Vallado, D. A., *Fundamentals of Astrodynamics and Applications*, Space Technology Series, McGraw Hill, New York, 1997.
- [5] Chobotov, V., *Spacecraft Attitude Dynamics and Control*, Krieger Publishing Company, Malabar, Florida, 1991.
- [6] Lefferts, E. J., Markley, F. L., and Shuster, M. D., “Kalman Filtering for Spacecraft Attitude Estimation,” *Journal of Guidance, Control, and Dynamics*, Vol. 5, No. 5, Sep-Oct 1982, pp. 417–429.
- [7] Bar-Itzhack, I. Y. and Oshman, Y., “Attitude Determination from Vector Observations: Quaternion Estimation,” *IEEE Transactions on Aerospace and Electronic Systems*, , No. 1, Jan 1985, pp. 128–136.
- [8] Shuster, M. and Oh, S., “Three-Axis Attitude Determination from Vector Observations,” *Journal of Guidance and Control*, Vol. 4, No. 1, Jan-Feb 1981, pp. 70–77.
- [9] Musser, K. L. and Ebert, W. L., “Autonomous Spacecraft Attitude Control Using Magnetic Torquing Only,” *Flight Mechanics/Estimation Theory Symposium*, May 23-24 1989, pp. 23–38, NASA Conference Publication.
- [10] Wiśniewski, R., *Satellite Attitude Control Using Only Electromagnetic Actuation*, Ph.D. thesis, Aalborg University, Aalborg, Denmark, Dec 1996.
- [11] Wiśniewski, R., “Linear Time Varying Approach to Satellite Attitude Control Using Only Electromagnetic Actuation,” *AIAA Guidance Navigation and Control Conference, New Orleans, LA*, August 11-13 1997.
- [12] Makovec, K. L., *A Nonlinear Magnetic Controller for Three-Axis Stability of Nanosatellites*, Master’s thesis, Virginia Polytechnic Institute and State University, Blacksburg, Virginia, July 2001.

- [13] Meirovitch, L., *Methods of Analytical Dynamics*, McGraw-Hill, Inc., New York, 1988.
- [14] Nguyen, D. and Widrow, B., “Neural Networks for Self-Learning Control Systems,” *IEEE Control Systems Magazine*, Vol. 10, No. 3, April 1990, pp. 18–23.
- [15] Hyland, D. C. and King, J. A., “Neural Network Architectures for Stable Adaptive Control, Rapid Fault Detection and Control System Recovery,” *Advances in the Astronautical Sciences*, Vol. 78, 1992, pp. 40–424, Proceedings of the 15th Annual Rocky Mountain Guidance and Control Conference. Keystone, CO, USA.
- [16] Vadali, S., Krishnan, S., and Singh, T., “Attitude Control of Spacecraft Using Neural Networks.” *Advances in Astronautical Sciences*, Vol. 82, No. 1, Feb 1993, pp. 271–286, Proceedings of the AAS/AIAA Spaceflight Mechanics Meeting held February 22-24, 1993, Pasadena, California.
- [17] Rodriguez, G. R. and Puig-Suari, J., “Applications of Neural Networks to the Satellite Attitude Control Problem,” *Advances in Astronautical Sciences*, Vol. 97, No. 1, 1998, pp. 963–982.
- [18] Omidvar, O. and Elliot, D. L., *Neural Systems for Control*, Academic Press, San Diego, CA, 1997.